

Document downloaded from:

<http://hdl.handle.net/10251/121778>

This paper must be cited as:

Roig-Flores, M.; Simicevic, F.; Maricic, A.; Serna Ros, P.; Horvat, M. (2018). Interfacial Transition Zone in Mature Fiber-Reinforced Concretes. *ACI Materials Journal*. 115(4):623-631. <https://doi.org/10.14359/51702419>



The final publication is available at

<http://doi.org/10.14359/51702419>

Copyright American Concrete Institute

Additional Information

INTERFACIAL TRANSITION ZONE IN MATURE FIBER

REINFORCED CONCRETES

Marta Roig-Flores ^{1,2*} (marroifl@upv.es), Filipa Šimičević ³ (filipa.simicevic@gmail.com),

Ana Maričić ³ (ana.maricic@oblak.rgn.hr), Pedro Serna ¹ (pserna@cst.upv.es) & Marija

Horvat ⁴ (mhorvat@hgi-cgs.hr)

*Corresponding author

¹ Institute of Concrete Science and Technology (ICITECH), Universitat Politècnica de València (UPV), Camino de Vera, 46021, València, Spain

² Eduardo Torroja Institute for Construction Science, Spanish National Research Council (CSIC-IETcc), Calle de Serrano Galvache, 4, 28033 Madrid, Spain

³ Faculty of Mining, Geology and Petroleum Engineering, University of Zagreb, Pierottijeva 6, 10000 Zagreb, Croatia

⁴ Croatian Geological Survey, Department of Geology, Sachsova 2, 10000 Zagreb, Croatia

Biography:

Marta Roig-Flores received her BEng+MEng in Civil Engineering, MSc in Concrete Engineering, and PhD in Construction Engineering, from *Universitat Politècnica de València* in 2013, 2015 and 2018, respectively. She is currently working as a research assistant at Eduardo Torroja Institute for Construction Science from the Spanish National Research Council (CSIC-IETcc). Her research interests include special types of concrete, self-healing, fiber-reinforced, self-compacting, refractory concrete, etc.

Filipa Šimičević is a MEng student in Geology at Faculty of Mining, Geology and Petroleum Engineering of University of Zagreb in Croatia. She received her BEng in Geology at the

University of Zagreb in 2014. She has been admitted as an exchange student through Erasmus program at the Institute of Concrete Science and Technology in spring 2016 and the research carried out at UPV is presented in this paper.

Ana Maričić is Assistant Professor of Geology at Faculty of Mining, Geology and Petroleum Engineering at University of Zagreb in Croatia. She received PhD in 2014 at the same institution. Her main scientific interest is in determination of deposits, properties, durability to weathering and usability of natural and crushed stone and sand and gravel for construction purposes.

Pedro Serna is Full Professor at Universitat Politècnica de València (UPV), Spain. He holds a PhD in Civil Engineering from UPV and Ecole Nationale des Ponts et Chaussées, France (1984). His main research area is special types of concrete: fiber-reinforced (FRC), high strength, self-compacting, etc. Prof. Serna has collaborated in the sections of the Model Code and Spanish EHE on FRC, is Chairman of SC5-CTN83 and RILEM TC-CCF and member of WG11 and CEN-TC-104.

Marija Horvat is a Research Associate at Croatian Geological Survey and Assistant Professor at Faculty of Mining, Geology and Petroleum Engineering of University of Zagreb in Croatia. She received the B.Sc. in Geology (Mineralogy and Petrology) at the University of Zagreb in 1995 and the Ph.D. in the field of Geology (Petrology and Geochemistry) at Eötvös Loránd University in Budapest in 2005. Her main research fields consider minerals and rocks.

ABSTRACT

The Interfacial Transition Zone (ITZ) in concrete is the region of the cement paste that is disturbed by the presence of an aggregate or fiber. This work focuses on the ITZ around silica and dolomite grains and steel fibers. The analysis performed is based on: the macroscale properties of the specimens; petrographic analyses with polarized microscopy; and qualitative and quantitative SEM analyses. The following types of concrete were tested: standard quality (SQ); high-quality with steel fibers (PFRC); and Ultra High Performance Fiber Reinforced Concrete (UHPRFC). The most important parameters affecting ITZ are: the properties of the disturbing elements and the mix composition of the concrete. In PFRC, a differentiated zone of thickness 20 μm (787.40 μin) was observed around a dolomite grain, showing a preferential growth of Ca-based compounds. In UHPRFC, SEM-EDS analysis revealed CSH of lower Ca/Si ratios in the proximity of fibers and aggregates.

Keywords: fiber-reinforced concretes, aggregates-cement paste ITZ boundary, fiber-cement paste ITZ boundary, calcium silica hydrates.

INTRODUCTION

Concrete is a highly heterogeneous, porous, multiphase material whose essential components are aggregates and bulk cement paste. The Interfacial Transition Zone (ITZ) is the zone of the cement paste that has been disturbed by the presence of the aggregate particle. ITZ is produced mainly by the “wall effect”, produced by the inefficiency of cement particles suspended in mix water to pack together when they are in the close vicinity of a much larger solid object, such as aggregate particles [1, 2]. Other factors may also influence ITZ, such as chemical reactions at the aggregate/fiber surface (as produced by the epitaxy) and larger heterogeneities due to micro-bleeding and void formation.

The ITZ is usually a narrow region with a thickness around $50\ \mu\text{m}$ ($1968.5\ \mu\text{in}$) [3, 4] that has proportionally less cement particles and more water than other regions of the cement paste [5]. Because of this higher amount of water, concrete porosity in the ITZ is higher compared to that in the bulk of the hardened paste. The relatively large dimension of the spaces remaining between the paste and the aggregates leads to preferential crystallization of hydrates corresponding to the most mobile ions, ettringite and portlandite [4, 2]. In the case of Ultra High Performance Concrete (UHPC), the ITZ has been detected to be around $4\ \mu\text{m}$ ($157.48\ \mu\text{in}$) [5].

ITZ are considered to influence concrete properties [6] due to their higher porosity when compared with the surrounding cement paste, producing a potential weak zone around aggregates that could affect both concrete strength and durability. In UHPC, this durability concern is considered negligible [5]. Some studies [7] have highlighted the importance of these boundaries by detecting Alkali-Silica gels filling not only microcracks and pore voids, but also the cement paste/aggregate boundary. This is a concern regarding the long-term properties of the material.

Several studies agree on the importance of the grain size distribution of aggregates and cement in ITZ. The size of the ITZ is thought to increase for concretes with higher amount and larger size of the aggregates [6, 8], and it is also affected by their geometrical characteristics [9]. The density of the ITZ has been reported to be affected by the water/cement ratio of the mix, with lower w/c ratios leading to less porous ITZ and higher presence of anhydrous particles [8, 10]. Some cross interactions have been reported between the density of ITZ and aggregate size, since reducing aggregate size decreased the porosity of ITZ for aggregates of size 150-300 μm (5905.5-11811 μin) but not for those of size 2.36-4.76 mm (0.093-0.187 in) [8, 10]. Moreover, differences between the mechanical properties of aggregate and paste may lead to tension concentrations in the boundary [11], producing microcracking and changing the properties of the ITZ. The presence of mineral additions can also affect ITZ: adding blast furnace slag [12] has been reported to increase the Si/Ca ratios near the unhydrated slag core, and adding condensed silica [4] produced an ITZ of a more homogeneous and denser microstructure. Different types of aggregates can also affect the properties of ITZ, such as recycled aggregates [13] or lightweight aggregates [11, 14].

There is some agreement that ITZ do not drastically influence the mechanical properties of concrete. This effect may be of great influence, however, in the case of fiber-reinforced cement composites and their long-term properties [9], due to the importance of bond strength in the tensile behavior of fiber-reinforced concrete, and then, of the fiber-paste ITZ [15].

RESEARCH SIGNIFICANCE

Most of the studies from the literature regarding ITZ focus on one type of concrete, or a same concrete family with little variations. The authors believe that a same study dealing with different fiber-reinforced concrete families is of interest for the concrete field. In this work, the presence, size and composition of ITZ have been analyzed in three types of concrete:

standard quality concrete (so-called in this work standard quality “SQ” concrete), high quality concrete with steel fibers (precast fiber-reinforced “PFRC” concrete), and Ultra High-Performance Fiber Reinforced Concrete (“UHPRFC”). For each type of concrete, the ITZ was studied around steel fibers and two kinds of aggregates (silica and dolomite). Thus, a total of 9 combinations were considered.

EXPERIMENTAL PROCEDURE

The three types of concrete have been analyzed using: (i) their macroscale properties; (ii) a petrographic analysis with polarized microscopy in thin sections; and (iii) Scanning Electronic Microscopy (SEM) using Energy-Dispersive X-ray Spectroscopy (EDS) detectors.

Materials

The concrete samples investigated in this study were prepared at *Universitat Politècnica de València*. Their main constituents are cement, tap water, aggregates, mineral additions and admixtures. **Table 1** shows the composition of the three concrete types: Standard Quality concrete (SQ), Precast FRC concrete (PFRC), and Ultra-High Performance Fiber-Reinforced Concrete (UHPRFC).

SQ concrete was prepared using CEM II/A-V 42.5 R, which contains fly ash and displays rapid acquisition of strength. The water/binder ratio was 0.53. As for the aggregates, the coarser aggregate used was calcareous, with maximum size 20 mm (0.787 in), and the sand used for preparation was mixed sand siliceous-calcareous of size 0-4 mm (0-0.157 in).

PFRC concrete was prepared using CEM I 42.5 R, which which does not contain additions and displays rapid acquisition of strength. The water/binder ratio was 0.45. As for the aggregates, the coarser aggregate used was calcareous, with maximum size 12 mm (0.472 in), and the sand used for preparation was mixed sand siliceous-calcareous of size 0-4 mm (0-0.157 in). Limestone powder (Omya Clariana) was added as filler fraction. The steel fibers

added are macrofibers BEKAERT Dramix 65/35 BN.

UHPFRC was prepared using CEM II/A-V 42.5 R. The water/binder ratio was 0.17. As for the aggregates, the sand used for preparation silica sand of size 0-2 mm (0-0.079 in). Filler fractions silica fume (Elkem 940-U) and quartz flour (Quarzfin U-S500) were added. Reinforcement was obtained using. The steel fibers added are microfibers with a diameter of 0.2 mm (0.008 in) and 13 mm (0.512 in).

Tap water was used in all three types of concrete, with a pH around 7 (checked with pH strips). Superplasticizer was used in all concretes: Sika ViscoCrete 5980 in SQ and PFRC, and Sika ViscoCrete 225P in UHPFRC.

Concrete casting

The specimens were casted in molds, demolded the following day, and stored afterwards in a humidity chamber for 28 days. Uniaxial compressive strength at 28 days was determined with three cylindrical specimens $\Phi 150 \times 300$ mm ($\Phi 5.906 \times 11.811$ in) for types SQ and PFRC, and with three cubes with an edge of 100 mm (3.937 in) for UHPFRC, according to EN 12390-3 [16]. The reason for this difference, owes to the much higher strength of UHPFRC, which can exceed the limits of the testing equipment and makes sample preparation (capping/polishing) considerably harder. In UHPFRC, 100 mm cubes have been reported as providing similar compressive strength as 150 mm cubes [19]. Workability was also assessed with slump test EN 12350-2:2009 for types SQ and PFRC, and slump-flow EN 12350-8 for UHPFRC [17, 18].

Petrographic analysis

Macroscopic and microscopic observations were performed to determine the mineralogical composition of sand and gravel fraction and the textural features of concrete. These tests were ran at the Faculty of Mining, Geology and Petroleum Engineering, University of Zagreb, and the Croatian Geological Survey. Photomicrographs were taken with a Zeiss Axio

Lab. A1 HAL 35 petrographic microscope equipped with a digital camera.

Virgin concrete specimens of each batch were used to collect samples for this study. In preparation for the test, the specimens were sawed into thin sections and then glued on glass using Canadian balsam. After sawing, the thin sections were polished using Al_2O_3 powder. The standard thickness of the thin sections was up to 0.03 mm (1181.1 μm) measured after the polishing phase. The thin sections were observed in the microscope, and afterwards, following Evamy & Shearman method [20], the thin sections of SQ and PFRC concrete types were painted with an Alizarin red S and K-ferricyanide solution for easy differentiation of carbonate minerals (calcite and dolomite).

SEM analyses

The equipment used for Scanning Electron Microscopy was a JEOL JSM 6300 at the Electron Microscopy Service from *Universitat Politècnica de València* (**Fig. 1** left). Three detectors were used: Backscattered Electron Detector (BSE, JEOL), X-ray Detector (EDS, Oxford Instruments), and Secondary electron detector (SE, JEOL).

Virgin specimens of each concrete type were used to collect samples for this study. Concrete specimens were left to mature in humidity chambers until the age of six months old, when they were sawed into smaller pieces and roughly polished to remove sharp fiber terminations from the surface to obtain the samples for the analyses. The small samples were manually polished with sandpaper of progressively decreasing grading. After polishing, the samples were dried for 4 hours in an oven at 60°C (140°F) to remove their humidity. Since concrete has low conductivity, the samples were given a carbon coating treatment with BAL-TEC SCD 005, which deposits a fine layer of carbon (transparent to the electron beam but conductive) on the surface of the samples. Afterwards, the samples were stored in a low vacuum recipient and glued on conductive carbon films on metal plates for the electron microscopy. A thin layer of conductive liquid silver paint (colloidal silver) was used to

connect the metal support with the sample (**Fig. 1** right).

SEM-BSE analyses were made to locate the paste, fibers and aggregates, since darker grey tones indicate lighter elements. Line scans and mappings showed qualitatively the general predominance of combined calcium and silica in different proportions, followed by aluminum, which corresponds with the cement paste. The presence of aggregates was reflected as peaks of calcium with absence of silica for limestone grains and vice-versa for silica grains. Steel fibers were identified in the locations with strong iron peaks. After using SEM-BSE to locate the aggregates and decide on the points of interest, they are quantitatively analyzed with SEM-EDS. SEM-EDS analyses were performed at different distances from the boundary (orthogonal to the aggregate or fiber surface). Results from points in the paste were gathered at three distance levels from the boundary: 5-10 μm , 20-40 μm and 50-80 μm (0.197-0.394 in, 0.787-1.575 in and 1.969-3.150 in, respectively). These distances were chosen due to the reported presence of ITZ around 50 μm (0.197 in) in the literature [3, 4]. In the case of UHPFRC, since its ITZ was expected to be smaller as reported in the literature [5], and due to its smaller aggregate size, some additional analyses were made at a distance from the boundary of around 0.5-1.1 μm (19.69-43.31 μin).

EXPERIMENTAL RESULTS AND DISCUSSION

Macroscopic properties

UHPFRC had the highest uniaxial compressive strength in cubes of 156.50 MPa (22.70 ksi) measured in 100-mm cubes, which have been reported to similar equivalent strength as 150-mm cubes. The compressive strengths of SQ and PFRC types were equivalent to C35/45 and C45/55 concrete classes respectively, following the cylinder/cube denomination from EN 206:2013 (**Table 2**). These strengths were between 3.4 and 2.8 times lower than those of UHPFRC. This was due to their composition, mainly their cement content and water/binder

ratio. Slump tests were carried on all three types of concrete specimens, showing similar results for SQ and PFRC types and self-compactability for UHPFRC.

Petrographic description of samples

Pictures obtained from the concrete thin sections described are presented in **Fig. 2**.

In SQ concrete (**Fig. 2a** and **Fig. 2b**), differences in grain size were observed, corresponding to gravel and sand components/fractions mixed in concrete. Gravel pebbles were round with sizes between 3 mm (0.118 in) and 7 mm (0.276 in), and sand grains were mostly angular with sizes between 0.1 mm (0.0039 in) and 0.5 mm (0.0197 in). Among gravel pebbles, limestone fragments predominate; additionally, one metamorphic rock fragment and some quartzite fragments were observed as well. The sand grains were mainly quartz, with small amounts of carbonate (limestone) grains. Among sand components, two small grains of mica with high interference color were also observed. The difference in color of cement near the grains (darker or brighter zones) is not evident (**Fig. 2a**). **Fig. 2b** shows SQ thin section stained with Alizarin Red S and K-ferricyanide and covered with coverslip. The “wall effect” around the aggregates is present as an inefficient packing of neighbor aggregate grains. In fact, aggregates were generally surrounded by cement paste and were not in direct contact with other aggregates. In that part of the sample, aggregates of size around 1.5 mm (0.059 in) were surrounded by an area of around 60 μm (2362.2 μin) where only grains of size smaller than around 15 μm (590.55 μin) could be found. The ITZ between the fiber and the cement paste was not visible. Microcracks were visible within the pebbles of limestones. Some of them were filled with cement paste, indicating that cracks occurred before or during mixing.

The analyses on PFRC concrete specimens (**Fig. 2c** and **Fig. 2d**) also revealed round gravel and angular sand fragments, as in SQ concrete. The composition of gravel and sand fragments was also similar to that of SQ concrete (quartz and limestone), with the main difference being the size of the (aggregates): gravel pebbles had sizes between 2.5 mm (0.098

in) and 6 mm (0.236 in); sand fragments had sizes from 0.2 mm (0.0079 in) to 1 mm (0.0394 in). The black circular area in **Fig. 2c** corresponds to a steel fiber. The examined thin section showed no evident difference in color in the cement paste near the grains (darker or brighter zones) and there was no visible reaction between fiber and cement. Around the fiber, visible aggregate particles are located at a distance higher of 15 μm (590.55 μin), showing a “wall effect” around the fibers. Dolomite grains were also detected, since calcite grains were stained in red after applying the solution of Alizarin Red S and K-ferricyanide, while dolomite grains were not stained (**Fig. 2d**).

UHPFRC has a visually more uniform composition than SQ and PFRC (**Fig. 2e** and **Fig. 2f**). Allotriomorphic monomineral quartz grains with sizes between 0.125 mm (0.005 in) and 1.5 mm (0.059 in) were predominant, with some polymetamorphic quartz and quartzite grains. Subangular forms of all type of grains were evident (**Fig. 2e**). In the cement paste microlites of quartz flour could be recognized. The cement paste color is darker than in SQ and PFRC because of the silica fume. Unlike in SQ and PFRC, zones of brighter color could be found around most quartz grains and steel fibers. This coloring was likely produced by a preferential location of quartz grains around aggregates and fibers. The thickness of this colored layer varies from approximately 30 μm (1181.1 μin) around the fibers and approximately 10 μm (393.70 μin) around the aggregates (**Fig. 2f**). Microcracks filled with cement paste were detected within the quartz grains.

SEM-EDS analyses

ITZ around silica grain in SQ concrete

EDS analyses were performed at different distances from the boundary. The measurement points for the analyzed SQ concrete sample are marked on **Fig. 3**. The presence of different compounds has been analyzed in terms of atomic percentage and distance from the interface in μm . All the points in the SQ concrete sample showed similar composition and proportion

of elements, Calcium and Silica being the most significant, without a clear difference in the ITZ. In the analysis, only those points with significant amount of Ca and Si have been analyzed, using 3% as the threshold. The Ca/Si ratio of the points analyzed remained between 0.55 and 3.5. The most frequent CSH had an atomic Ca/Si ratio around 1.5, which corresponds with the Ca/Si ratio of Jennite, $\text{Ca}_9(\text{Si}_6\text{O}_{18})(\text{OH})_6 \cdot 8\text{H}_2\text{O}$.

Some of the points diverged from these common trends. Three points (37, 40 and 43) had Ca/Si ratios around 3.00, indicating the presence of unhydrated cement particles in the Alite form, Ca_3SiO_5 . Furthermore, the upper row of measurement points (44-48), those at least 80 μm (3149.6 μin) from the boundary, showed different compositions than the rest. Points 45, 46 and 47 had a high content of aluminum and silica (Si/Al atomic ratios of 3.33, 3.27 and 3.24, respectively) but less than 1% calcium content. Points 44 and 48, conversely, had significantly higher calcium content.

ITZ around silica grain in PFRC concrete

In this case, in contrast with results of standard quality concrete, the composition of paste around the silica grain (**Fig. 4**) showed a predominance of Ca around the aggregate, while Si content remained almost constant and under 5% of atomic percentage. Calcium presence was high in all the points of this concrete type, which indicated a significant amount of portlandite-calcite type compounds. The most common Ca/Si atomic ratio was approximately 3.00, indicating the predominance of Alite. The second most common compound was Jennite (points with Ca/Si close to 1.5).

ITZ around dolomite grain in PFRC concrete

Several calcareous grains and some dolomite grains were detected in the precast quality concrete. The ITZ was analyzed around one of them (**Fig. 5**). The high presence of calcium compounds was much more noticeable in this case than for SQ concrete, with calcite/portlandite compounds around the boundary, especially at points 15, 17, 34 and 35.

Figure 5 right indicates a decrease of the Ca/Si ratio with distance to the grain, with the trend changing partially for distances higher than 20 μm (787.40 μin). The different composition of the paste around the dolomite grain showed a favored location of compounds with similar composition to the aggregate (related with epitaxy). This was evidence of the presence of an ITZ around the dolomite grain.

ITZ around steel fiber in PFRC concrete

The points of analysis around a steel fiber in PFRC concrete are shown in **Fig. 6**. The values of the atomic Ca/Si ratio were more homogeneous in this case than around silica and dolomite aggregates, and ratios remained generally under 5.00. Most of the ratios were around 3.00, which indicating the presence of Alite. Also common were points with a Ca/Si ratio around 1.50 and 2.00, indicating the presence of Jennite and Belite, Ca_2SiO_4 . The presence of Alite and Belite indicated in turn the presence of unhydrated cement particles around the steel fiber, which were not detected around aggregates in this type of cement.

ITZ around silica grain in UHPFRC

The selected Si grain and the analyzed points are displayed in **Fig. 7**. The majority of points have Ca/Si ratios under 1.00, owing to their high content in silica. Most of the values gathered around 1.00, 0.80 and 0.50, which suggested the presence of Tobermorite $\text{Ca}_5\text{Si}_6\text{O}_{18}\text{H}_2$, or Plombierite $\text{Ca}_5\text{H}_2\text{Si}_6\text{O}_{18}\cdot 6\text{H}_2\text{O}$ for values close to 0.80. Plombierite is a specific type of Tobermorite, with 14 \AA of basal spacing, which is the most hydrated type of Tobermorite [21]. Other CSH compounds may have formed due to the high dosages of silica fume additions and the presence of fly ash in the mix of this type of cement. The values are homogeneous and no evidence of an ITZ has been detected in this case.

Since all the aggregates in the considered UHPFRC were silica based, there were no dolomite grains to analyze to compare with SQ and PFRC.

ITZ around steel fiber in UHPFRC

UHPFRC contained very large amounts of steel fibers, which were also smaller than the

fibers in PFRC concrete. The points of analysis around a steel fiber in this type of concrete are shown in **Fig. 8**. Like the results around the silica grain for UHPFRC, the Ca/Si values around the steel fiber were very low, around 0.50 or even lower (**Fig. 9**). However, in concordance with the results around the PFRC concrete, several points have Ca/Si ratios around 2.00 or 3.00, which indicates the presence of Belite or Alite, i.e., unhydrated cement particles. The results are very homogeneous and no presence of ITZ has been detected.

Effect of element proximity

In order to discard any undue bias or influence of the proximity of the aggregate or fiber on the SEM-EDS analyses, the concentration of Mg, for the dolomite aggregate, and Fe, for the steel fiber were evaluated. These results were easier to interpret than representing Ca or Si, which are the dominant compounds in the paste. The results of this analysis of Mg and Fe have been shown in **Fig. 10** for PFRC concrete. The concentrations of these elements remained generally under 1% in atomic percentage, showing no relation with the distance to the element. Thus, the measurements had no bias by its near location. This lack of bias was also present in the other concrete types, including UHPFRC for the closest distances.

Influence of concrete type on the composition of the ITZ

The composition of the cement paste was similar for standard and precast concrete (**Fig. 11**), and yet the precast concrete cement paste showed higher presence of portlandite and calcite type compounds and slightly higher presence of Calcium Aluminate Silica Hydrates (CASH) than the standard concrete specimens. These two types of concrete had the same types of aggregates, and so the differences in the composition of the paste came from the type of cement and w/c ratio. Using pure CEM I cement as in the precast concrete type produces a higher number of Ca-based compounds while CEM II cement with fly ash, as in the standard concrete type, will produce a higher presence of CSH gels and less portlandite, and thus higher percentages of silica. The composition of the paste for UHPFRC differs from the other

two samples, showing CSH with lower Ca/Si ratios, as suggested by Gatty et al. [22], and other compounds of higher silica percentage.

Fig. 12 represents the silica versus calcium distribution, depending on the type of concrete and boundary element. All the samples followed the same inverse trend (silica decreased when calcium increased, with a slope of approximately -1), independently of the composition of their boundary element. Moreover, each type of concrete followed a slightly different behavior: the composition of the paste for PFRC concrete presented higher calcium content; the one for UHPFRC presented higher silica content; and the one for the SQ concrete showed a broader distribution.

Discussion

In this work, the “wall effect” has been detected with the different microscopy techniques. ITZ was observed as alterations of the composition trends of the paste with SEM-EDS. The ITZ were significant only around the analyzed dolomite aggregates, and their thickness has been estimated at around 20 μm (787.40 μin). The widths of the detected ITZ were smaller than the 50 μm (1968.5 μin) as mentioned in the literature [3, 4], but this difference can be produced by the high hydration degree of the samples, as proposed by Kong [23]. In contrast with the results of Ollivier et al. [2], no preferential presence of ettringite in the ITZ was noticed in this study, and all concretes had very marginal contents of sulfur.

In the case of UHPFRC, polarized microscopy showed coloration differences around aggregates and fibers. This could have been produced by a preferential location of quartz fine fractions, as reported in some publications [24], but no ITZ in the cement paste has been detected. This is coherent with the bibliography, which indicates the ITZ of UHPFRC as denser and have negligible transport properties [5].

CONCLUSIONS

The following conclusions can be drawn from this study:

1. EDS analyses used in combination with SEM and microscopy of thin sections allow to detect the “wall effect” in all the considered concrete types by analyzing the composition of the cement paste around aggregates and fibers.
2. Standard concrete (SQ) showed only hydrated compounds, while precast concrete (PFRC) and UHPFRC had some points identified as unhydrated particles (Belite). In general, the most frequent compounds found were Calcium Silica Hydrates: Jennite, Plombierite and Tobermorite. UHPFRC had compounds with higher percentages of silica than the other concrete types, which can indicate the formation of CSH of lower Ca/Si ratios.
3. Alterations of the composition of the paste in the PFRC proximity of dolomite aggregates have been detected, showing higher percentage of calcium than around silica grains in those areas. This indicates a preferential location of Ca-based compounds around dolomite aggregates.
4. The ITZ around the fibers in the PFRC concrete is less scattered than in UHPFRC, while in the case of the aggregates both types of concrete have less dispersion than SQ.
5. The results obtained showed that the most important parameters affecting ITZ are the composition of the disturbing elements (grain/fiber) and their geometry and the mix composition of the concrete.

REFERENCES

1. K. Scrivener, "Characterization of the ITZ and its quantification by test method," in *Engineering and Transport Properties of the Interfacial Transition Zone in Cementitious*

Composites, RILEM Publications, 1999, pp. 3-14.

2. J. P. Ollivier, J. C. Maso and B. Bourdette, "Interfacial Transition Zone in Concrete," Elsevier Science Inc, 1995.

3. G. Prokopskia and J. Halbiniak, "Interfacial transition zone in cementitious materials," Cement and Concrete Research, vol. 30, pp. 579-583, 2000.

4. A. Bentur and M. D. Cohen, "Effect of Condensed Silica Fume on the Microstructure of the Interfacial Zone in Portland Cement Mortars," Journal of the American Ceramic Society, vol. 70, p. 738–743, 1987.

5. J. C. Scheydt and H. S. Müller, "Microstructure of Ultra High Performance Concrete (UHPC) and its Impact on Durability," in *Ultra-High Performance Concrete and Nanotechnology in Construction (Hipermat)*, Kassel, 2012.

6. H. Jennings and T. J. Jeffrey, "Materials of Cement Science Primer: The Science of Concrete," Infrastructure Technology Institute (ITI), Research and Innovative Technology Administration, 2009.

7. Š. Šachlová, R. Přikryl and Z. Pertold, "Alkali-silica reaction products: Comparison between samples from concrete structures and laboratory test specimens," *Materials Characterization*, vol. 61, no. 12, pp. 1379-1393, 2010.

8. Y. Gao, G. De Schutter, G. Ye, H. Huang, Z. Yu and K. Wu, "Investigation on the interfacial transition zone in ternary blended cement based composites with respect to curing age and water binder ratio," in *First International Conference on Concrete Sustainability*, Tokyo, 2013.

9. A. Bentur and M. G. Alexander, "A review of the work of the RILEM TC 159-ETC: Engineering of the interfacial transition zone in cementitious composites," *Materials and Structures/Materiaux et Constructions*, vol. 33, pp. 82-87, 2000.

10. A. Elsharief, M. D. Cohen and J. Olek, "Influence of aggregate size, water cement ratio and age," *Cement and concrete research*, 2003.
11. M. Husem, "The effects of bond strengths between lightweight and ordinary aggregate-mortar, aggregate-cement paste on the mechanical properties of concrete," *Materials Science and Engineering: A*, vol. 363, no. 1–2, p. 152–158, 2003.
12. M. Boháč and M. Gregerová, "The influence of blast-furnace slag hydration products on microcracking of concrete," *Materials Characterization*, vol. 60, no. 7, pp. 729-734, 2009.
13. I. del Bosque, W. Zhu, T. Howind, A. Matías, M. de Rojas and C. Medina, "Properties of interfacial transition zones (ITZs) in concrete containing recycled mixed aggregate," *Cement and Concrete Composites* 81 (2017), vol. 81, pp. 25-34, 2017.
14. P. Vargas, O. Restrepo-Baena and J. I. Tobón, "Microstructural analysis of interfacial transition zone (ITZ) and its impact on the compressive strength of lightweight concretes," *Construction and Building Materials*, vol. 137, p. 381–389, 2017.
15. D.-Y. Yoo, S.-T. Kang, J.-H. Lee and Y.-S. Yoon, "Effect of shrinkage reducing admixture on tensile and flexural behaviors of UHPFRC considering fiber distribution characteristics," *Cement and Concrete Research*, vol. 54, pp. 180-190, 2013.
16. EN 12390-3:2009 Testing hardened concrete - Part 3: Compressive strength of test specimens.
17. EN 12350-2:2009 Testing fresh concrete - Part 2: Slump-test.
18. EN 12350-8:2010 Testing fresh concrete - Part 8: Self-compacting concrete - Slump-flow test.
19. B. Graybeal and M. Davis, "Cylinder or Cube: Strength Testing of 80 to 200 MPa (11.6 to 29 ksi) Ultra-High-Performance Fiber-Reinforced Concrete, " *ACI Materials Journal*, vol. 105, no.6, p. 603-609, 2008.

20. Ewamy B. D. and D. J. Sherman, "The application of chemical staining techniques to the study of diagenesis in limestones," *Proc. Geol. Soc. London*, vol. 1599, pp. 102-103, 1962.
21. E. Bonaccorsi, , S. Merlino, A.R Kampf, "The crystal structure of tobermorite 14 Å (plombierite), a C–S–H phase, " *Journal of the American Ceramic Society*, vol. 88, no. 3, pp. 505-512, 2005.
22. L. Gatty, S. Bonnamy, A. Feylessoufi, C. Clinard, P. Richard and H. Van Damme, "A transmission electron microscopy study of interfaces and matrix homogeneity in ultra-high-performance cement-based materials," *Journal of materials science*, vol. 36, no. 16, pp. 4013-4026, 2001.
23. Y. Kong, P. Wang, S. Liu, G. Zhao and Y. Peng, "SEM Analysis of the Interfacial Transition Zone between Cement-Glass Powder Paste and Aggregate of Mortar under Microwave Curing," *Materials*, vol. 9, no. 9, p. 733, 2016.
24. M. Courtial, M.-N. de Noirfontaine, F. Dunstetter, M. Signes-Frehel, P. Mounanga, K. Cherkaoui and A. Khelidj, "Effect of polycarboxylate and crushed quartz in UHPC: Microstructural investigation," *Construction and Building Materials*, vol. 44, pp. 699-705, 2013.

TABLES AND FIGURES

List of Tables:

Table 1 – Composition of concrete mixtures

Table 2 – Compressive strength and slump results

List of Figures:

Fig. 1 – SEM Equipment JEOL JSM 6300 at the Electron Microscopy Service from Universitat Politècnica de València (left) and sample prepared in the metal support shown with the liquid silver paint (right).

Fig. 2 – Thin sections micrographs for concrete SQ (a), PFRC (c) and UHPFRC (e, f) and colored thin section for SQ (b) and PFRC (d) concretes.

Fig. 3 – Points analyzed by EDS on SQ concrete around a silica grain and Ca/Si ratios.

Fig. 4 – Points analyzed by EDS on PFRC concrete around a silica grain and Ca/Si ratios.

Fig. 5 – Points analyzed by EDS on PFRC concrete around a dolomite grain and Ca/Si ratios.

Fig. 6 – Points analyzed by EDS on PFRC concrete around a steel fiber and Ca/Si ratios.

Fig. 7 – Points analyzed by EDS on UHPFRC around a silica grain and Ca/Si ratios.

Fig. 8 – Points analyzed by EDS on UHPFRC around a steel fiber.

Fig. 9 – Ca/Si ratios on concrete UHPFRC around a steel fiber.

Fig. 10 – Mg (left) and Fe (right) around the dolomite aggregate and fiber for the PFRC concrete.

Fig. 11 – Distribution of atomic Al/Ca and Si/Ca ratios for the three types of concrete. Circle marks correspond to SQ concrete, cross-stitch to PFRC and triangles to UHPFRC.

Fig. 12 – Si vs Ca distribution for the three types of concrete and the three types of boundary. Circle marks correspond to SQ concrete (C1), cross-stitch to PFRC (C2) and triangles to UHPFRC (C3).

Table 1– Composition of concrete mixtures

Quantity (kg/m ³)	Standard Quality Concrete	Precast Fiber-Reinforced Concrete	Ultra-High Performance Fiber-Reinforced Concrete
<i>Labelled as:</i>	<i>SQ</i>	<i>PFRC</i>	<i>UHPFRC</i>
Cement	300	350	800
Silica fume	-	-	175
Water	157.5	157.5	175
<i>(water/binder)</i>	<i>(0.53)</i>	<i>(0.45)</i>	<i>(0.17)</i>
Gravel (calcareous)	904	950	-
Sand (mixed) 0-4 mm	904	899	-
Sand (siliceous) 0-2 mm	-	-	855
Limestone powder (<63 μm)	-	50	-
Quartz flour (<63 μm)	-	-	225
Superplasticizer	3	6.3	10
Fibers	-	40	150

Table 2– Compressive strength and slump results

	SQ	PFRC	UHPFRC
Average compressive strength at 28 days, cylinders, f_{cm}	45.98 MPa 6.67 ksi	55.17 MPa 8.00 ksi	-
Average compressive strength at 28 days, cubes, $f_{cm,cube}$	-	-	156.50 MPa 22.70 ksi
Standard deviation of f_{cm}	2.98 MPa 0.43 ksi	0.60 MPa 0.08 ksi	1.78 MPa 0.26 ksi
Slump test	180 mm 7.09 in	80 mm 3.15 in	750 mm 29.53 in

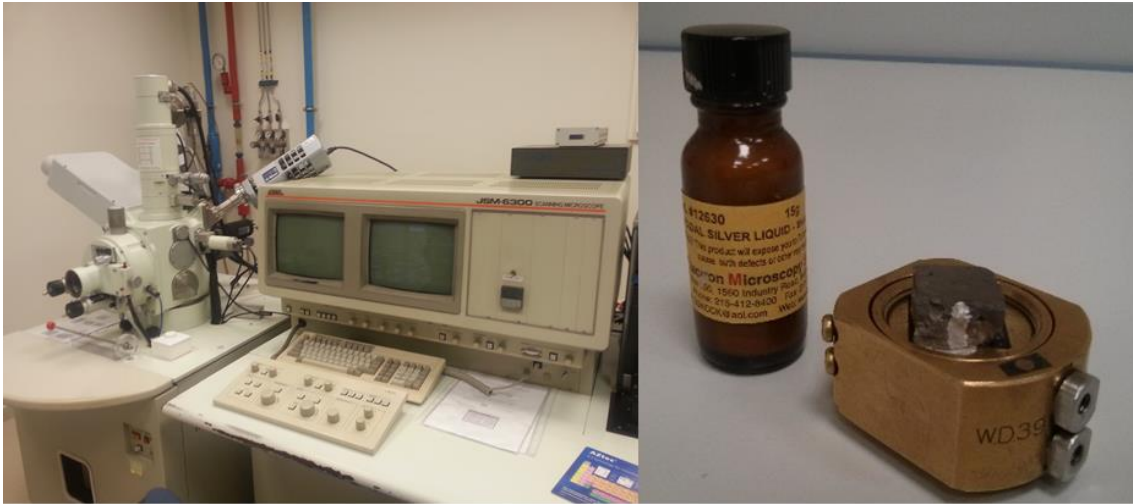


Fig. 1–SEM Equipment JEOL JSM 6300 at the Electron Microscopy Service from Universitat Politècnica de València (left) and sample prepared in the metal support shown with the liquid silver paint (right).

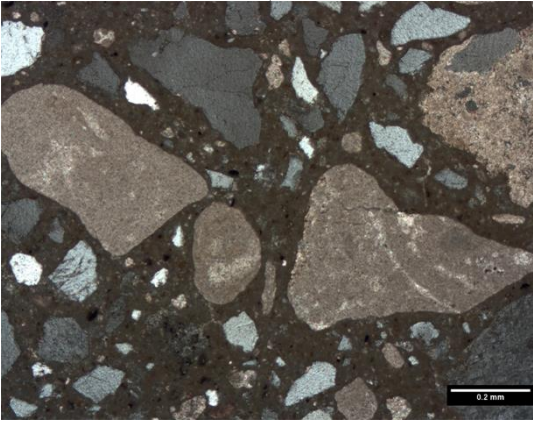
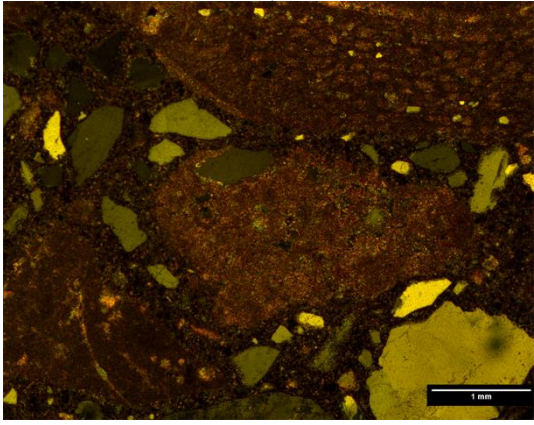
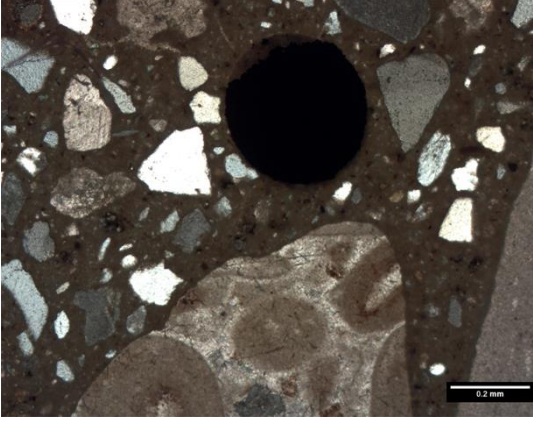
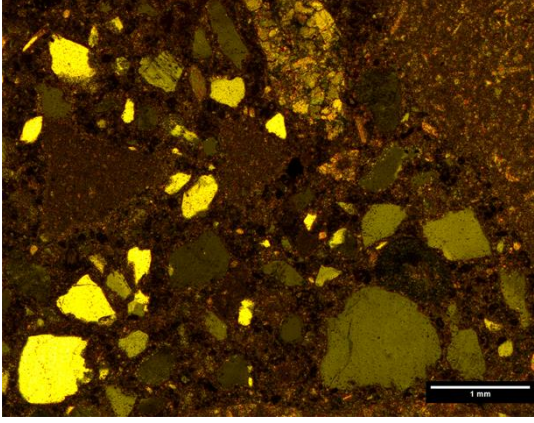
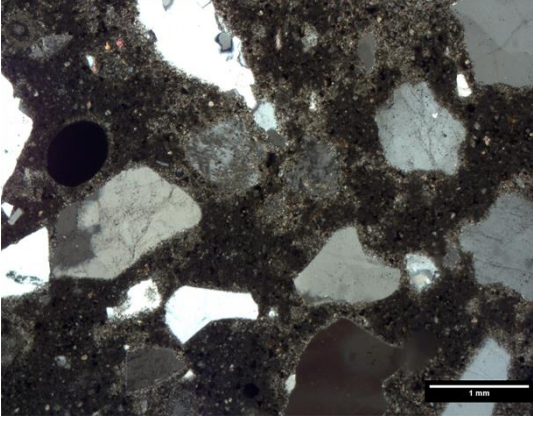
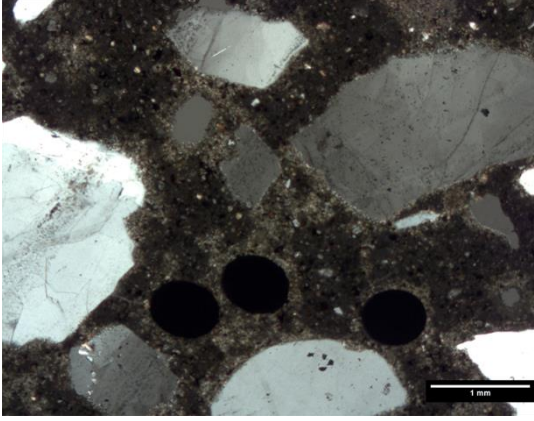
Type	Micrograph	Colored thin section
SQ	<p>a)</p> 	<p>b)</p> 
PFRC	<p>c)</p> 	<p>d)</p> 
UHPFRC	<p>e)</p> 	<p>f)</p> 

Fig. 2–Thin sections micrographs for concrete SQ (a), PFRC (c) and UHPFRC (e, f) and colored thin section for SQ (b) and PFRC (d) concretes.

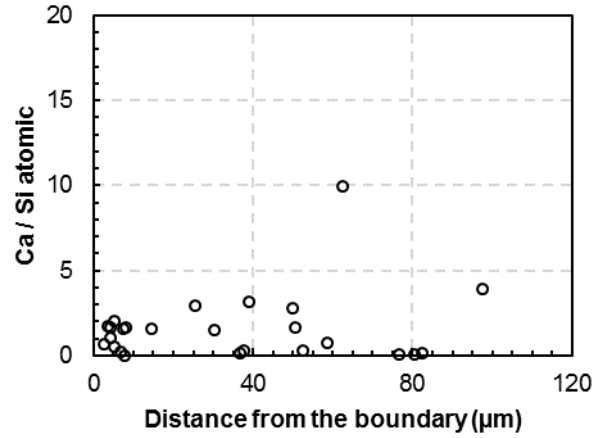
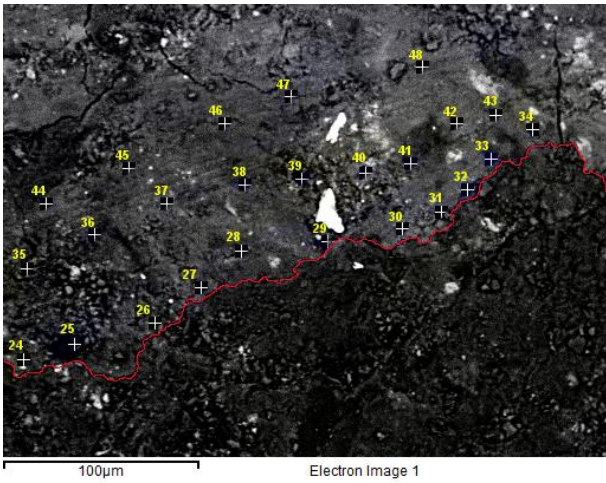


Fig. 3—Points analyzed by EDS on SQ concrete around a silica grain and Ca/Si ratios.

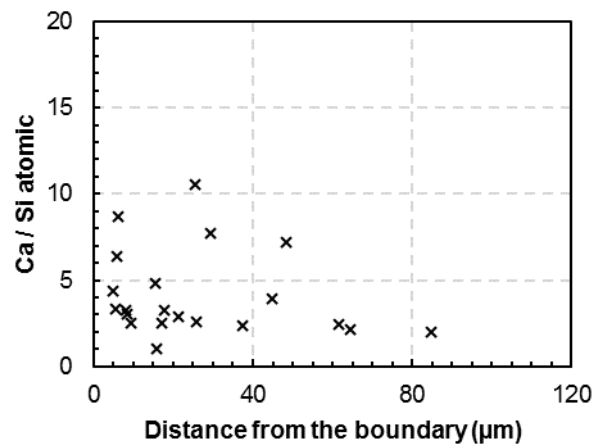
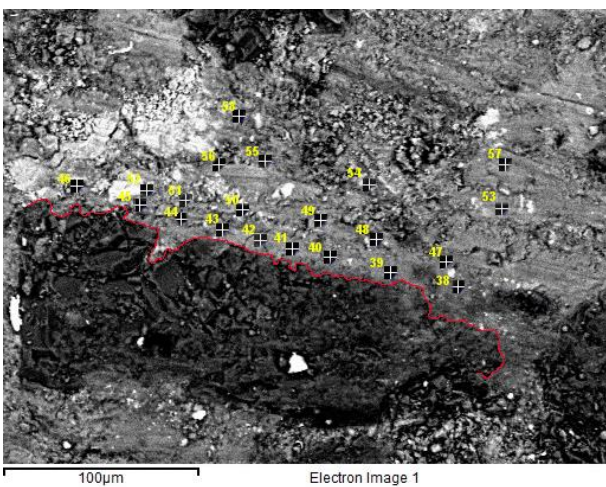


Fig. 4—Points analyzed by EDS on PFRC concrete around a silica grain and Ca/Si ratios.

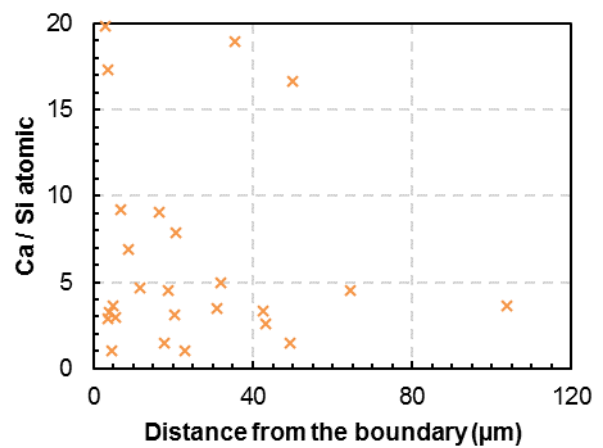
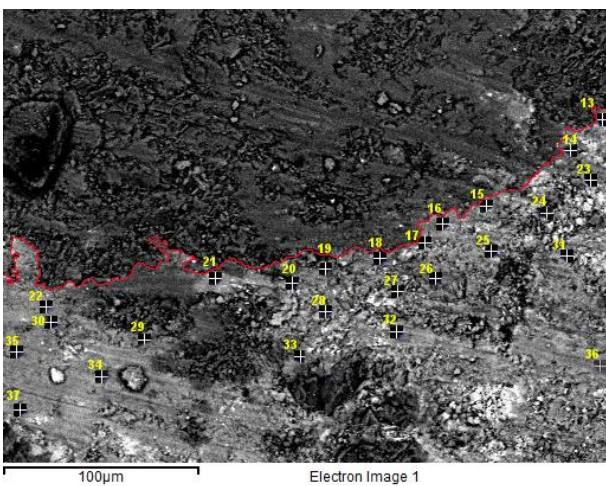


Fig. 5—Points analyzed by EDS on PFRC concrete around a dolomite grain and Ca/Si ratios.

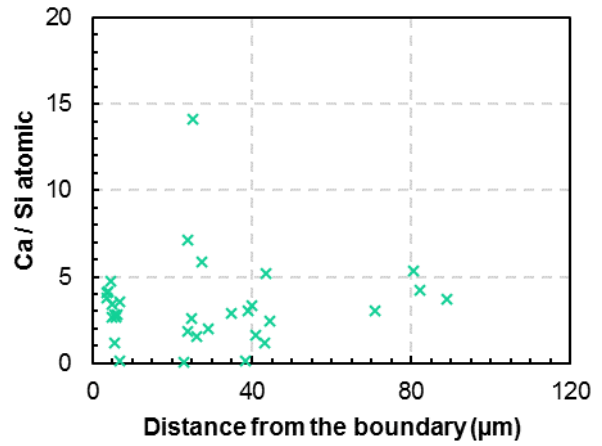
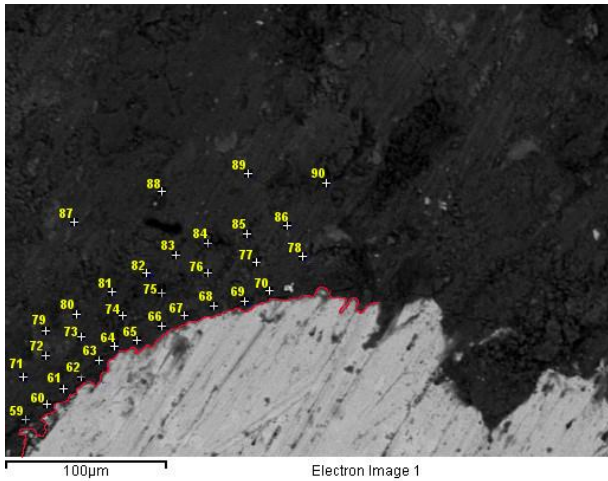


Fig. 6—Points analyzed by EDS on PFRC concrete around a steel fiber and Ca/Si ratios.

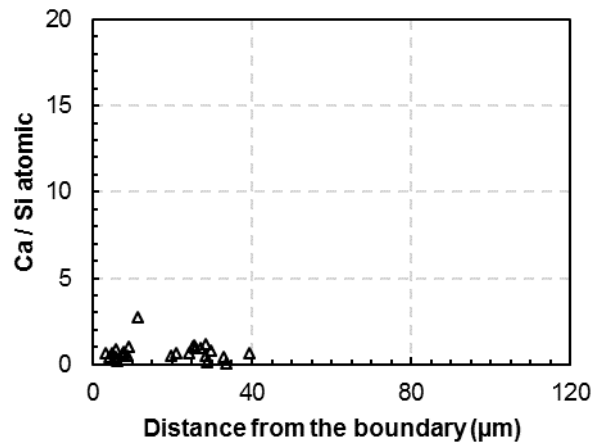
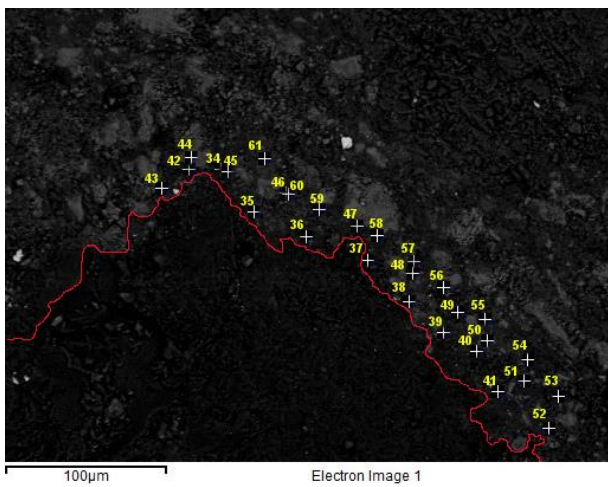


Fig. 7—Points analyzed by EDS on UHPFRC around a silica grain and Ca/Si ratios

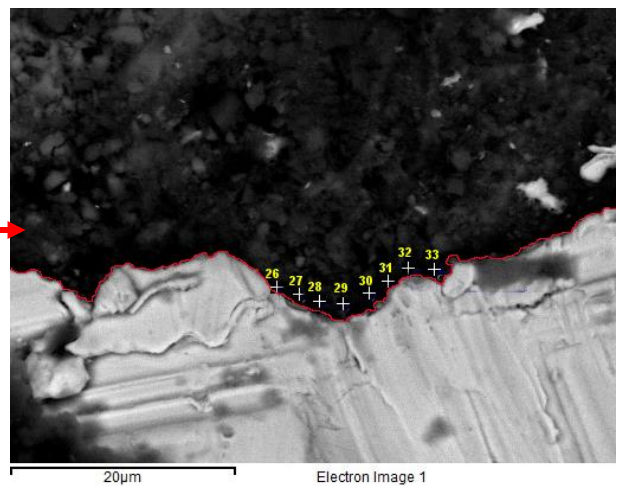
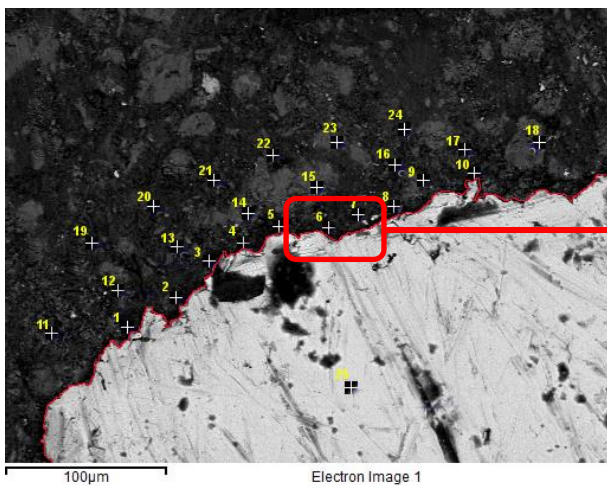


Fig. 8—Points analyzed by EDS on UHPFRC around a steel fiber.

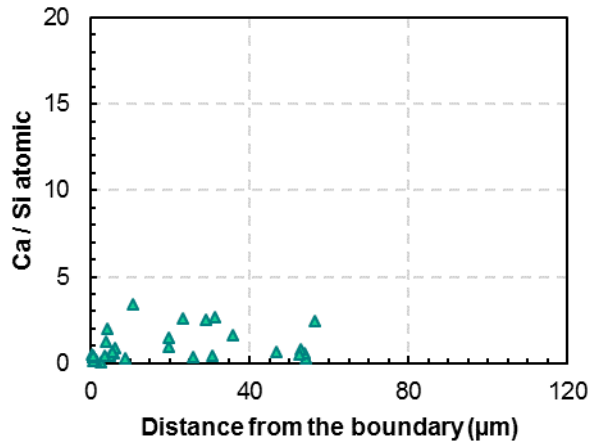


Fig. 9–Ca/Si ratios on UHPFRC around a steel fiber.

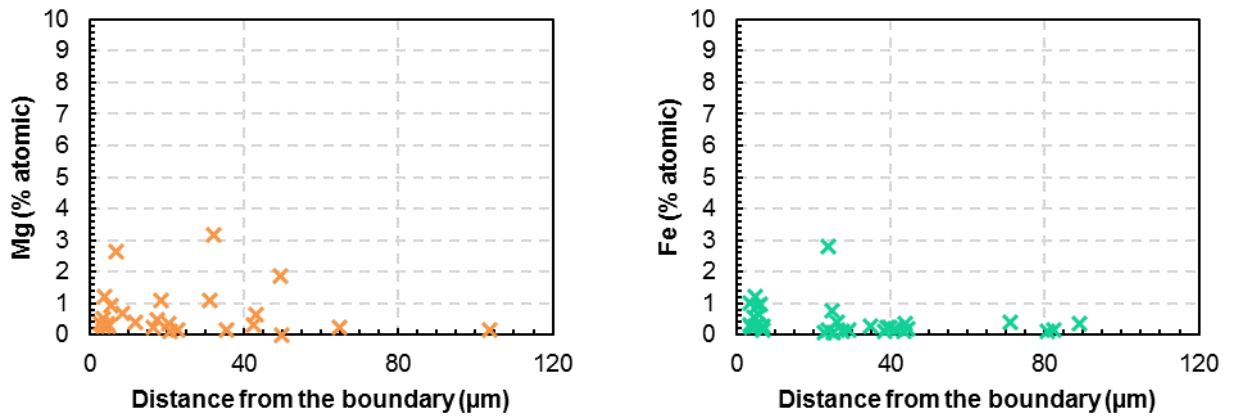


Fig. 10–Mg (left) and Fe (right) around the dolomite aggregate and fiber for the PFRC concrete.

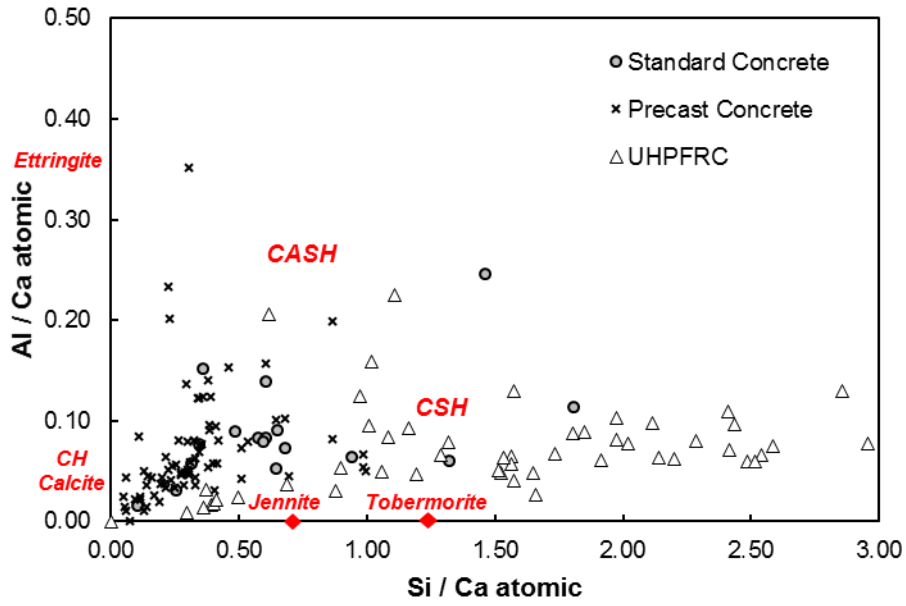


Fig. 11–Distribution of atomic Al/Ca and Si/Ca ratios for the three types of concrete. Circle marks correspond to SQ concrete, cross-stitch to PFRC and triangles to UHPFRC.

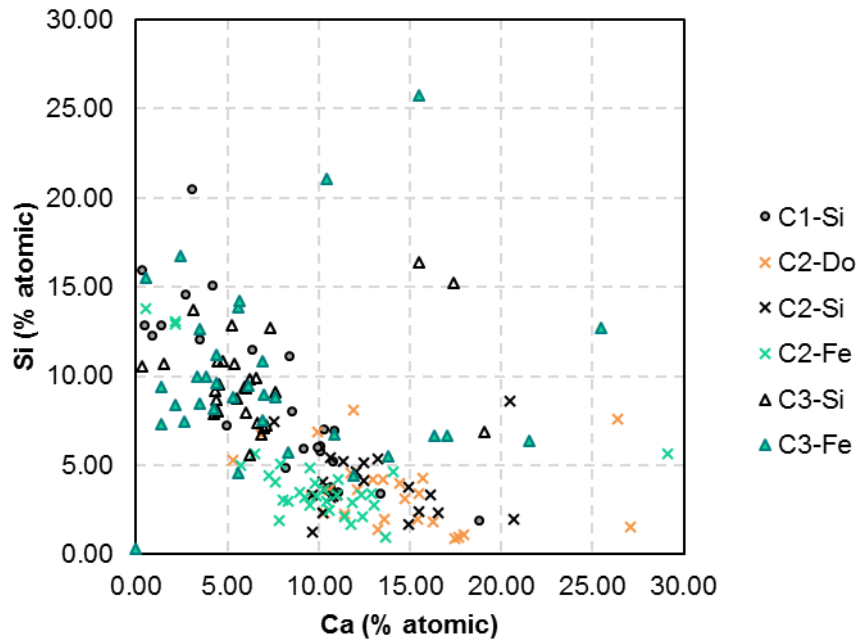


Fig. 12–Si vs Ca distribution for the three types of concrete and the three types of boundaries. Circle marks correspond to SQ concrete (C1), cross-stitch to PFRC (C2) and triangles to UHPFRC (C3).